https://doi.org/10.1038/s44183-025-00121-w

Offshore hydrogen production leaves a local hydrographic footprint on stratification in the North Sea

Nils Christiansen[1] ✉, Ute Daewel[1], Leopold Krings[2] & Corinna Schrum[1,3]

Offshore production of hydrogen powered by offshore wind energy offers a promising alternative to fossil fuels. However, current technologies return waste heat and brine into the sea, raising questions of potential effects on local and regional hydrography. This study evaluates the hydrographic footprint of offshore hydrogen in the context of anthropogenic pressures from offshore energy production, focusing on a scenario for the German Bight. Cross-scale modeling shows that waste heat emerges as the primary influence, causing temperature changes of up to 2 °C within 10's of meters around a 500 MW hydrogen plant. While tides prove to be decisive for the dilution of density plumes, we demonstrate that production capacity and discharge method determine the hydrographic footprint. Large-scale effects are minor and negligible compared to the impact of offshore wind farm wakes, however, waste heat can raise annual mean sea surface temperature by up to 0.2 °C near production sites.

As part of the global societal agenda to reduce carbon dioxide emissions, green hydrogen holds a pivotal role in decarbonizing the energy system. Given that electricity accounts for only 20% of global final energy consumption[1], primary renewable energy sources such as wind and solar power cannot meet the total global energy demand. Instead, green electricity must be converted into secondary energy sources such as hydrogen to keep the energy supply free of fossil fuels. Green hydrogen, which is generated from renewable energies, has several potential applications, e.g., for energy storage or to substitute coal, oil, and gas as energy sources for industrial needs or transportation. Consequently, there is high demand for green hydrogen in the global energy transition. For instance, the European Union has production targets of up to 10 million tons of green hydrogen by 2030[2], which corresponds to an output capacity of at least 40 GW, more than today's installed total offshore wind capacity in European waters[3].

Hydrogen can be produced by the electrolysis of water, i.e. by the chemical decomposition of water particles (H_2O) into hydrogen (H_2) and oxygen (O_2) using electrical energy. The demands on water resources and the availability of renewable electricity are well met by the production of hydrogen near offshore wind farms, which motivated recent research projects to investigate the feasibility and development of offshore hydrogen production (e.g., *Sea2H2*[4]; *OffsH2ore*[5]). While being a promising solution for green energy generation, offshore hydrogen production comes with significant water consumption, seawater desalination and the use of chemicals[6,7]. These processes generate by-products and high-saline brine that are currently intended to be released into the environment[4,5,8], which raises questions about the hydrographic footprint of offshore hydrogen and the ecological risks of potential future production.

There is little research, particularly modeling studies, regarding the effects of offshore hydrogen production on hydrodynamics to date. However, emerging processes can be assumed comparable to those associated with discharge of high-saline brine from freshwater production[9] or carbon storage reservoir management[10], which both include similar seawater treatment. In the Mediterranean Sea, salinity anomalies resulting from desalination discharge have been shown to propagate at kilometer scales and create density currents that can influence coastal water dynamics[9]. In a different study, Roberts et al.[11] emphasized the variability of the intensity of these brine plumes across spatial and temporal dimensions, reporting spatial variations between tens to hundreds of meters and temporal fluctuations over the tidal cycle. Dewar et al.[10] reinforced the tidal influence on brine dispersion for the North Sea, showing that brines dilute rapidly in hydrodynamically active regions. Plumes of critical concentration extended to scales of hundreds of meters or less, with the method of brine discharge having a significant influence on spatial dispersion. Consequently, discharge from hydrogen production in the North Sea is expected to be complex and determined by local hydrodynamic conditions.

[1]Institute of Coastal Systems – Analysis and Modeling, Helmholtz-Zentrum Hereon, Max-Planck-Straße 1, 21502 Geesthacht, Germany. [2]cruh21 GmbH, Ludwig-Erhard-Straße 1, 20459 Hamburg, Germany. [3]Institute of Oceanography, Center for Earth System Research and Sustainability, Universität Hamburg, Bundesstraße 53, 20146 Hamburg, Germany. ✉e-mail: nils.christiansen@hereon.de

In this study, we aim to explore the local processes associated with the discharge from offshore hydrogen production, with the goal of quantifying the hydrographic footprint of a hydrogen plant. Our focus lies on understanding how different disposal methods and production capacities influence hydrodynamic processes and compare the impact of hydrogen production to those of the offshore wind farms, in which they will be installed. In this context, we address how offshore hydrogen production might affect the hydrography and stratification patterns in the North Sea under a future renewable energy scenario in the German Bight. Density stratification plays a crucial role in ecosystem dynamics, as it determines the vertical transport of nutrients in the water column and thus the ecosystem productivity in the surface layers[12]. Consequently, perturbations caused by the release of heat and brine could become critical for lower trophic ecosystem dynamics and should be investigated in more detail. To evaluate the footprint of offshore hydrogen production, we use numerical modeling with nested unstructured grids, allowing to resolve both the local density plumes and the large-scale dynamics in the North Sea. Given the limited insights available on the industrial development of offshore hydrogen technologies, we closely align our assumptions with the report by Rudolph et al. (2023)[5].

In the following, we will explain the technology of offshore hydrogen production in more detail, before introduction the numerical model system and analyzing the model experiments.

Methods

Offshore hydrogen production

Various technologies are currently under development for offshore electrolysis, with the most promising being alkaline electrolysis (AEL) and proton exchange membrane electrolysis (PEMEL)[6,13,14]. These low-temperature electrolysis technologies demand high feed water purity and therefore require desalination of the seawater prior to the chemical decomposition. Thus, current hydrogen production at sea consists of three main processes: (i) desalination, (ii) electrolysis, and (iii) water treatment for system cooling on the platform (Fig. 1). These processes require large amounts of seawater and influence the hydrographic footprint of a production site, as they generate thermal and chemical by-products.

The main impact of an offshore hydrogen plant results from the seawater treatment for desalination and system cooling, similar to seawater desalination in the context of freshwater production. Methodologies for desalination can be grouped into membrane processes like Reverse Osmosis (RO), which are most prominently used in global seawater desalination but require advanced pretreatment against biofouling, and thermal processes like Multi-Effect Distillation (MED), which can produce feed water of higher purity but have higher energy and water demands[6,15].

In this study, we are focusing on the PEM electrolysis as proposed by Rudolph et al. (2023)[5], which demonstrates greater suitability for offshore applications than AEL[5,6]. Thereby, the PEMEL is combined with a MED unit for desalination, which uses a series of evaporators to produce distillate at low temperatures and allows for utilization of waste heat from the electrolysis to evaporate the seawater (https://www.veoliawatertechnologies.com/en/technologies/multiple-effect-distillation-med, accessed on June 3, 2024). During these steps, the MED is accumulating brine and heated seawater from the condenser, which are recirculated into the sea.

The extent of water consumption and by-products can vary significantly depending on the production technologies and the decline in electrolysis efficiency over time[5]. Additional variability due to environmental conditions complicates an accurate representation of the processes associated with offshore hydrogen production without industrial information. Therefore, we strongly simplify these processes here to assess the impact of the water consumption and discharge on the hydrodynamic environment.

The seawater mass balance of a single hydrogen platform can be divided into desalination and cooling water treatment. In this context, the demand for cooling water is notably higher than that for desalination, encompassing the entire platform's cooling requirements. Referring to

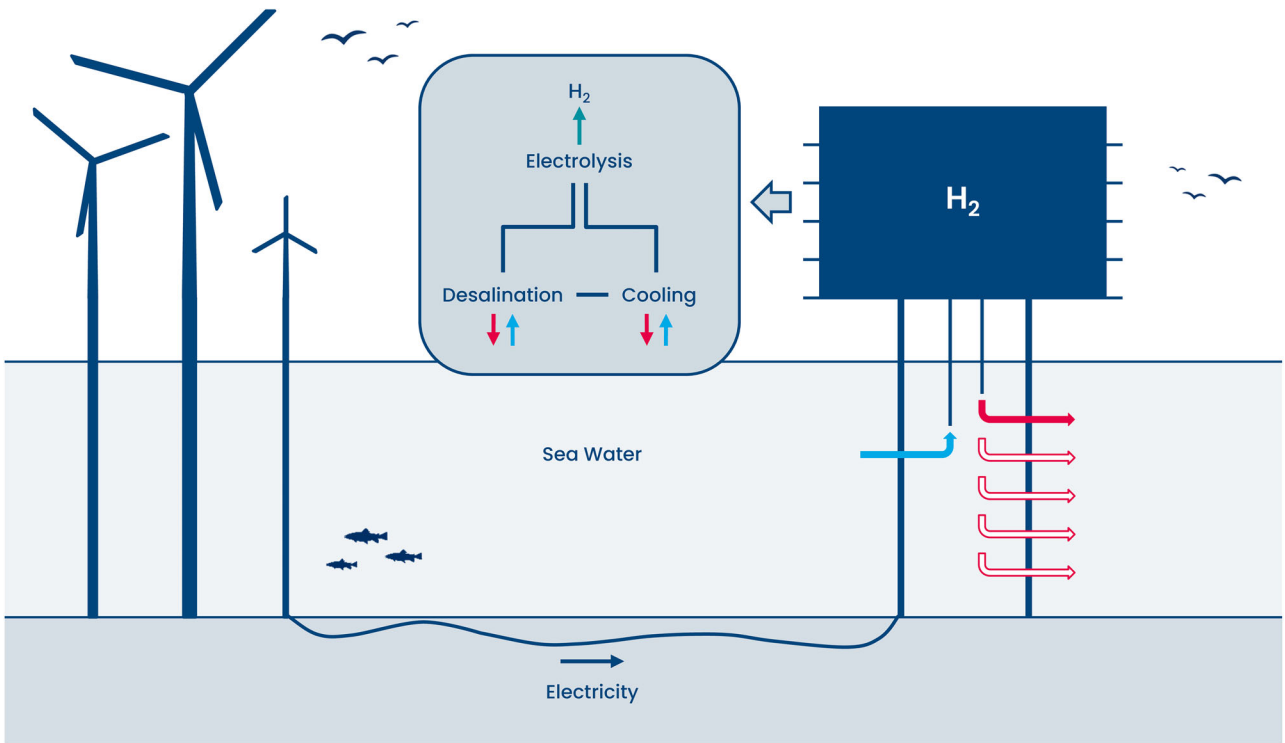

Fig. 1 | Illustration of the key processes involved in offshore hydrogen production. Seawater is extracted near the surface (light blue arrow) and utilized for cooling water treatment and desalination. Using electrical energy from offshore wind sources, the desalinated water is electrolized to produce hydrogen (H_2) as the final product. By-products and cooling water are returned to the sea near the surface (red arrow) or alternatively distributed over depth or near the bottom (white arrows). The figure is based on the report by Rudolph et al. (2023)[5]. The gray, centered box highlights the processes taking place on the platform.

Rudolph et al. (2023)[5], the cooling water treatment circulates about 86,400 m^3 of seawater per day, equating to an average inflow and outflow of 3,600 $m^3\ h^{-1}$. In addition, assuming constant seawater inflow over time, the MED unit requires a volume flux of 915 $m^3\ h^{-1}$ to produce 32 $m^3\ h^{-1}$ of distillate and generates an associated outflow of 748 $m^3\ h^{-1}$ of seawater from the condenser and 135 $m^3\ h^{-1}$ of brine (see Table 1). These values are based on the assumption of a 100 MW PEM electrolysis operating at full capacity and are scalable with the electrolysis capacity, as the platforms are designed as modular stacks[5].

SCHISM model description and setups

To examine the impact of offshore hydrogen production on ocean dynamics, we conducted cross-scale baroclinic ocean simulations with the three-dimensional ocean model SCHISM (https://github.com/schism-dev/schism). The SCHISM model system solves the Reynolds-averaged Navier-Stokes equations under hydrostatic and Boussinesq approximations using a semi-implicit finite-element/finite-volume method[16]. Turbulence is calculated using the Generic Length-Scale formulation[17] and the $k-\varepsilon$ model. Built on an unstructured horizontal triangular grid, SCHISM facilitates flexibility in local grid refinement, allowing for simultaneous resolution of large-scale ocean circulation and small-scale processes in designated focus areas. More detailed descriptions of the SCHISM model and its capabilities are given in Zhang et al. (2016[16]; 2016[18]).

Our study focuses on the central and southern North Sea region and specifically the development of offshore renewable energies in the German Exclusive Economic Zone (EEZ). We employed different model setups with varying grid resolutions to conduct a comprehensive analysis of the research domain. Essentially, we used a regional setup (*REGIO*) covering the entire study area to investigate cross-scale effects, and two local setups (*NEST5*, *NEST80*) nested within the regional setup to examine small-scale dynamics within tens of meters around hydrogen plants (Fig. 2).

The regional setup was initialized by and built upon validated North Sea simulations previously introduced in Christiansen et al.[19]. It is externally driven at its boundaries by daily mean ocean physics reanalysis data for the North-West European Shelf provided by the EU Copernicus Marine Service (https://doi.org/10.48670/moi-00059, downloaded February 2023). Atmospheric forcing is obtained from the coastDat-3 hourly hindcast dataset[20], while daily river discharge is derived from the mHM model[21]. Tidal amplitudes and phases from the HAMTIDE model[22] are prescribed at the model boundaries for eight tidal constituents (M_2, S_2, K_2, N_2, K_1, O_1, Q_1, P_1) and simulations are performed with a time step of 120 s. Meanwhile, the nested setups are controlled by the stored fields of the regional simulations via a one-way exchange of hourly boundary data. Validation of the nested model setups can be found in the Supplementary Material A.

The horizontal and vertical grid resolution used for the regional setup are adapted compared to the initial model by Christiansen et al.[19]. Here, the horizontal grid spacing varies between 700 m in shallow coastal areas (depth < 5 m) and 2000 m in the open sea (depth > 20 m). In rare cases, grid spacing is refined to 100 m to resolve small rivers at the land boundaries. Designated areas for offshore renewable energy are limited to a grid resolution of 500 m near the polygons and 1000 m within a radius of 10 km. The vertical grid has a maximum of 46 layers and is discretized with flexible Localized Sigma Coordinates[23].

The two nested setups are located within the model domain and are centered around the development area *SEN-1*, an area designated for

Table 1 | Volume flux rates and discharge concentrations from offshore electrolysis (100 MW) using PEMEL and MED technologies (obtained from Rudolph et al.[5])

	Inlet / Outlet	Volume Flux Rate	T	ΔT	S	ΔS
IN	Desalination	915 $m^3\ h^{-1}$	20 °C	-	35	-
	Cooling	3600 $m^3\ h^{-1}$	20 °C	-	35	-
OUT	Desalination	748 $m^3\ h^{-1}$	36 °C	16 °C	35	-
	Brine	135 $m^3\ h^{-1}$	42 °C	22 °C	45	10
	Cooling	3600 $m^3\ h^{-1}$	35 °C	15 °C	35	-

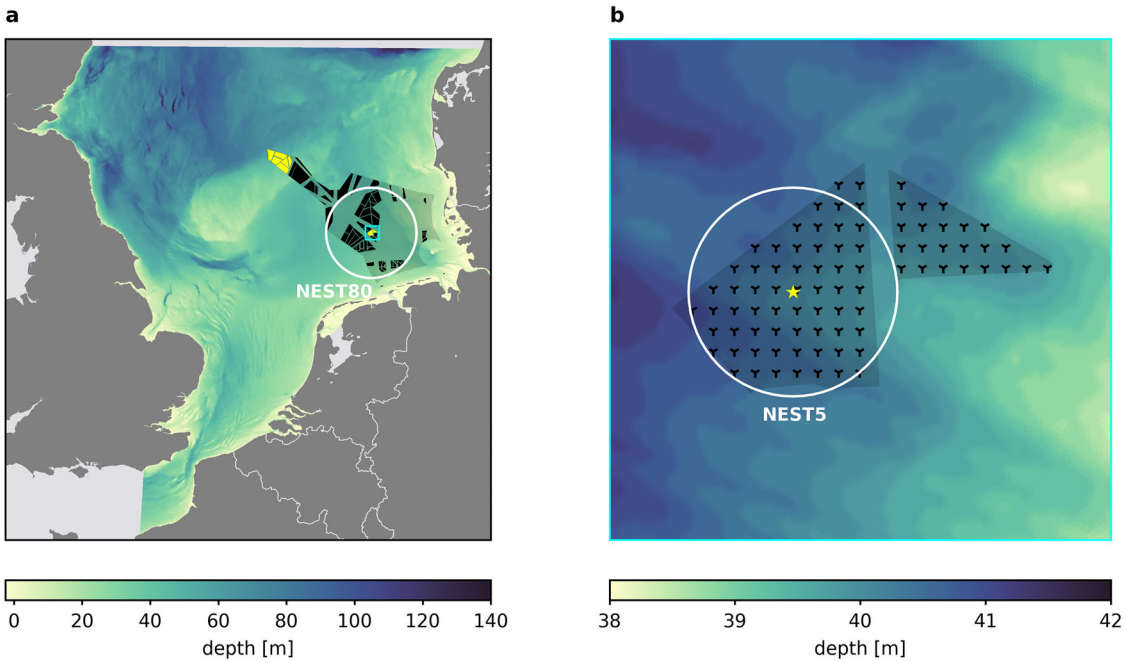

Fig. 2 | Model area and bathymetry of the hydrodynamic simulations. a Domain of the regional North Sea setup including the locations of offshore wind farms in the German Exclusive Economic Zone. The black polygons indicate the potential wind farms of the 2050 Scenario in the German Bight, with yellow polygons being designated for offshore hydrogen production. The white circle represents the domain of the nested setup NEST80 surrounding the wind farm SEN-1. The cyan rectangle indicates the zoomed-in view in panel **b**. **b** The development area SEN-1, with the yellow star indicating the hypothetical location of the H_2 electrolyzer and the black markers representing hypothetical wind turbine locations with a spacing of 1000 m. The nested setup NEST5 is highlighted by the white circle. Offshore wind farm information have been obtained from https://www.4coffshore.com/windfarms/.

Table 2 | List of model setups used in this study, sorted by temporal and spatial resolution (dt, dx) at offshore energy production sites

H_2 Simulations						
Model Setup	**dt [s]**	**dx [m]**	**Simulation Period**	**H_2 Scenario**	**H_2 Capacity [GW]**	**Discharge Level**
NEST5	2	10	2 days	*SEN-1*	0.5	Surface
NEST80	20	100	7 days	*SEN-1*	0.5	Surface, Bottom, Mix
REGIO (SEN1)	120	500	3 months	*SEN-1*	0.5, 1, 2, 5, 10, 20	Surface
REGIO (DE2050)	120	500	1 year	10 GW	Individual*	Surface
OWF Simulations						
Model Setup	**dt [s]**	**dx [m]**	**Simulation Period**	**OWF Scenario**	**OWF Capacity [GW]**	**OWF Effects**
REGIO (SEN1)	120	500	3 months	*SEN-1*	1**	Wind, Turbulence
*REGIO (DE2050)****	120	500	1 year	10 GW, 70 GW	Individual*,***	Wind + Turbulence

Simulations are divided into hydrogen (H_2) and wind farm (OWF) scenarios.
*capacities obtained from 4 C Offshore data (https://www.4coffshore.com/windfarms/).
**capacities are not considered in the wind and turbulence parameterizations. Data only used for turbine locations.
***offshore hydrogen production is considered in this simulation (as specified above for *DE2050*).

German offshore hydrogen production (https://aquaventus.org/en/projekt/aquasector/). These setups are intended for resolving the processes in the vicinity of hydrogen platforms at higher temporal and spatial resolution and to investigate natural and numerical dilution of discharge concentrations. The nested setups have a circular shape with a radius of 80 km and 5 km, respectively, around a hypothetical platform in the center of the *SEN-1* area (Fig. 2b). The temporal and spatial resolution are set to 20 s and 100–500 m and 2 s and 10–50 m, respectively, with grid cell sizes decreasing from the open boundary towards the center.

All model setups used in this study allow for consideration of the physical effects of offshore wind farms on hydrodynamics. The wind farm effects include the reduction in surface wind speed as well as the drag and turbulence induced by monopile foundations, for which parameterizations have been adopted from Christiansen et al.[19] and Christiansen et al.[24] respectively. Recent studies showed that offshore wind farms cause notable disturbances in ocean circulation and stratification themselves[19,24–28], and thus should be accounted for when studying the impact of offshore hydrogen production.

Implementation of offshore hydrogen production

To account for the seawater circulation and the discharge from the water treatment, volume changes and tracer concentration changes are implemented as additional sources and sinks in the numerical model, based on the existing point source implementation in *SCHISM*. Here, we used the estimated volume flux rates from Rudolph et al.[5] for the uptake and outflow and the waste heat and brine. After conversion from fluxes, the net volume changes $\triangle V$ are applied directly to the total water column volume at each model time step, which is calculated by

$$V_1 = V_0 + N_c \left(V_{outlet} - V_{uptake} \right) \tag{1}$$

$$\Delta V = V_1 - V_0 = N_c (V_{outlet} - V_{uptake}) \tag{2}$$

with V_0 and V_1 being the original and new value of the considered volume, V_{outlet} and V_{uptake} representing volumes from seawater uptake and discharge, and N_c as the capacity scaling factor relative to the 100 MW reference.

Changes in tracer concentrations $\triangle C$ are added at each time step to the tracer values at the respective discharge depths. As per Rudolph et al. (2023)[5], seawater uptake is presumed at ten-meter depth and discharge at five meters. Here, we concentrate on temperature and salinity changes caused by waste heat and brine, which are given in Table 1 ($\triangle T$ and $\triangle S$), and neglect chemical by-products. Assuming that the water density and specific heat remain constant in the model, the calculations for the tracer concentration changes are as follows:

$$C_1 V_1 = C_0 V_0 + N_c C_{outlet} V_{outlet} \tag{3}$$

$$\Delta C = C_1 - C_0 = N_c (C_{outlet} - C_0) \frac{V_{outlet}}{V_1}, \tag{4}$$

where C_1 is the new tracer value, C_0 is the original tracer value of the former time step, $(C_{outlet} - C_0)$ represents the changes in model tracers (ΔT and ΔS), V_0, V_{outlet} are the associated volumes defined in Eq. (1), and V_1 represents the sum of the volumes.

Tracer changes are considered for each outlet individually, with the fixed differentials ΔT and ΔS being added to the simulated tracer values at each time step and applied in the grid cell located closest to the hydrogen plant. For all simulation, we assumed constant volume flux rates over time at full capacity of the electrolysis.

Model experiments

A series of experiments were carried out to examine the spreading of the released waste heat and brine, including different hydrogen production scenarios and reference simulations for all three model setups (see Table 2). For each hydrogen scenario, we initiated with a presumed electrolysis capacity of 500 MW ($N_c = 5$) and defined seawater uptake and discharge at 10 m and 5 m depth, respectively. Discharge of temperature and salinity was assumed constant over time and was interpolated to the time steps of the simulations.

Most of the experiments focus on hydrogen production in the development area *SEN-1*, which is situated at a water depth of about 40 m in the German Bight (Fig. 2). The simulations take place in stratified water conditions in June 2013, immediately after the onset of summer stratification, which is decisive for ecological processes in the North Sea[29]. Tidal currents near *SEN-1* exhibit a velocity magnitude of around 0.4 m s^{-1} during the simulations and oscillate from southeastern to southwestern direction during the tidal cycle.

We conducted 2-day simulations using the fine-scale nested model *NEST5* to understand local dynamics of the temperature and salinity anomalies near the discharge location. The small-scale nested model *NEST80* was employed for 7-day simulations to assess the impact of different discharge depths on local density stratification. These scenarios included discharge of temperature and salinity near the surface (5 m), discharge near the bottom (35 m), discharge of temperature near the surface (5 m) and discharge of salinity near the bottom (35 m), discharge distributed vertically across all layers, and discharge near the surface spatially distributed to two discharge locations with distance of about 10 km within the

SEN-1 area (5 m). Seawater uptake remained constant at 10 m across all scenarios.

In addition, we employed two model configurations for the *REGIO* setup to analyze the large-scale extent of discharge dispersion in the North Sea. The *SEN1* configuration focused on hydrogen production at the *SEN-1* area, while the *DE2050* configuration considered the anticipated offshore renewable energy development in the German Exclusive Economic Zone by 2050. In both model configurations, we considered finer grid discretization (~ 500 m) inside the designated renewable energy areas to provide higher resolution of the discharge effects. For *SEN1*, we conducted 3-month simulations (June-August 2013) to determine the regional impact of a single hydrogen production site and to quantify the importance of production capacity, assuming hypothetical values between 500 MW ($N_c = 5$) and 20 GW ($N_c = 40$). The discharge depth remained at 5 m, with seawater uptake at 10 m depth. The *DE2050* configuration was used for 1-year simulations (January-December 2013) to assess the impact of future offshore hydrogen production and its interaction with the offshore wind farm effects.

The suggested future scenario is based on German government legislations[30,31] and available offshore development areas provided by the 4C Offshore database (https://www.4coffshore.com/windfarms/). The scenario involves offshore wind installations with a capacity of 70 GW for electricity and additional 10 GW capacity for offshore hydrogen production (Fig. 2a). To meet these plans, we utilized all available existing and future development areas in German waters, totaling 70 GW, and added additional 10.5 GW based on published offshore area potential analysis[32]. We assumed offshore hydrogen production at the designated area *SEN-1* and in the development areas far offshore, as energy transmission via hydrogen pipelines proves to be more cost-effective than power cables at distances of more than 100 km[33].

For the parameterizations of wind farm effects, turbine locations were obtained from the 4C Offshore database, if available, or approximated based on the projected development areas in combination with a presumed turbine spacing of 1000 m. Furthermore, we assumed a wind speed reduction of 8% with a decay factor of 30 km and pile diameters of 8 m with a drag coefficient of 0.63, following Christiansen et al. (2022a)[19] and Christiansen et al. (2023)[24].

Results

Local dispersion of waste heat and brine

As it is released into the sea, the discharge from the hydrogen plant mixes with the seawater, thereby introducing additional heat and salt to the water column. During this process, the initial concentrations of waste heat and brine become diluted by the surrounding seawater. The combined discharge exhibits a temperature increase ($\triangle T$) of 15.38 °C and a salinity increase ($\triangle S$) of 0.30, with a flow rate of approximately 6.226 m^3/s for a production capacity of 500 MW. Assuming a steady reference volume (V_0) of 1 m^3 of seawater, the immediate changes in seawater temperature and salinity after one second can be calculated to be about 13.25 °C and 0.26, respectively (detailed calculations can be found in Supplementary Material B). In the model, however, these changes are further diluted by the numerical discretization. For example, given the grid volume containing the point source in *NEST5* ($V_0 = 62.64$ m^3), the model discretization of 10 m and 2 s yields theoretical changes of 3.06 °C and 0.06, underestimating the actual density anomalies by a factor of four or more. In practice, we observe magnitudes using *NEST5* that are even slightly below with the theoretical estimates (Fig. 3), which is related to the exchange between neighboring grid cells within the model and the additional seawater uptake that influences the water column at the production site.

When released into the seawater, the diluted concentrations remain confined to the near-surface layers at the discharge location, due to the higher volume fluxes associated with the waste heat, generating positive buoyancy fluxes (Fig. 3b, c). However, the density changes and magnitudes oscillate over time, which correlates with the tidal cycle. Thereby, variations in tidal current speed lead to density- and tide-dominated processes affecting the density anomalies, as previously highlighted by Dewar et al. (2022)[10]. At high- and low-tide, when the tidal velocities are lowest, the changes in temperature and salinity become strongest, with magnitudes up to 1.9 °C and 0.04, respectively. During these periods, the dynamics are driven by local buoyancy, causing the density anomalies to rise to the sea surface (Fig. 3b, c) and creating strong upwelling at the discharge location (Fig. 3d). This vertical transport induced by the strong density gradients in the surface layers acts throughout the stratified water column and leads to excursions of the local pycnocline. In contrast, at high tidal velocities, tidal transport and mixing determine the local dynamics and cause horizontal dispersion and downstream advection of the signals. Consequently, temperature and salinity changes at the discharge location are smaller, with magnitudes of approximately 1.2 °C and 0.03 (Fig. 3b, c).

Over time, the discharge concentrations disperse throughout the water column, generating plumes that are transported by the tidal currents. For instance, a temperature plume at 5 m depth can exceed well beyond distances of 1000 m after continuous discharge over three hours and at tidal velocities of about 0.3 $m\ s^{-1}$ (Fig. 4a). In this context, the numerical resolution has a significant influence on the simulated magnitude of the plume, as the numerical dilution reduces the magnitude of the temperature and salinity signals. Here we observe that increasing the horizontal discretization from 10 m to 100 m or 500 m can result in a loss of 84% or 98% of magnitude information for the temperature plume at 500 MW, respectively (Fig. 4b, c). Moreover, the coarser grid increases the horizontal diffusion, causing the plumes to widen horizontally and affecting larger areas. It should be noted here that the numerical dilution depends not only on the grid size itself, but also on the exchange between neighboring grid cells and the volume of the discharge that is entered into the respective grid cell. An extrapolation of the numerical dilution at 500 MW capacity over the simulated 2-day period is depicted in Fig. 5.

As it is transported downstream, the diluted discharge experiences buoyancy forces and tidal mixing, which influence the spatial and vertical distribution of the temperature and salinity signals. Focusing on the sea surface, we find that the temperature and salinity anomalies behave similarly despite their different densities, indicating that the large amounts of waste heat dominate over the high salinity values of the brine (Fig. 6a, c). Their amplitudes and spatial extend can vary greatly depending on the tidal currents and the associated mixing (also seen in Fig. 3b, c). In Fig. 6a, c, we depict two examples of temperature and salinity plumes at different phases of the tidal cycle resolved with 10 m horizontal resolution. The signals oscillate horizontally around the discharge point with changing tidal direction and can extend more than 2000-3000 m from the source with strong tidal currents. Here, the plumes are exposed to two primary tidal directions, southeastern and western.

Averaged over the 2-day simulation, the density plumes form anomalies around the discharge site that are characterized by the tidal flow (Fig. 6b, d). Thereby, the strongest changes remain closely to the source. Here, we depict the maximum temperature and salinity changes over depth, which again look similar for temperature and salinity in direct vicinity to the discharge site. Considering a 500 MW capacity, we detect temporally averaged changes of approximately 0.1 °C and 0.002 within a radius of about 200 m. The strongest changes manifest within a radius of 50 m around the discharge point, with a significant increase in surface temperature of up to 1.85 °C near the source (Fig. 6b) and changes in salinity of about 0.037 (Fig. 6d). While the latter are considered less substantial, the changes in temperature exceed the natural interannual variability in monthly-mean surface temperature, which has been shown to vary from year to year by about 1 °C in the southern North Sea[34].

Offshore discharge scenarios

Discharge from offshore hydrogen production has been suggested in surface layers to reduce the impact of high temperatures on the water column[5]. In fact, the discharge depth proves to be critical for the impact of offshore hydrogen. In the present simulations, a weak vertical density stratification can be observed near *SEN-1* at the beginning of June, which is characterized

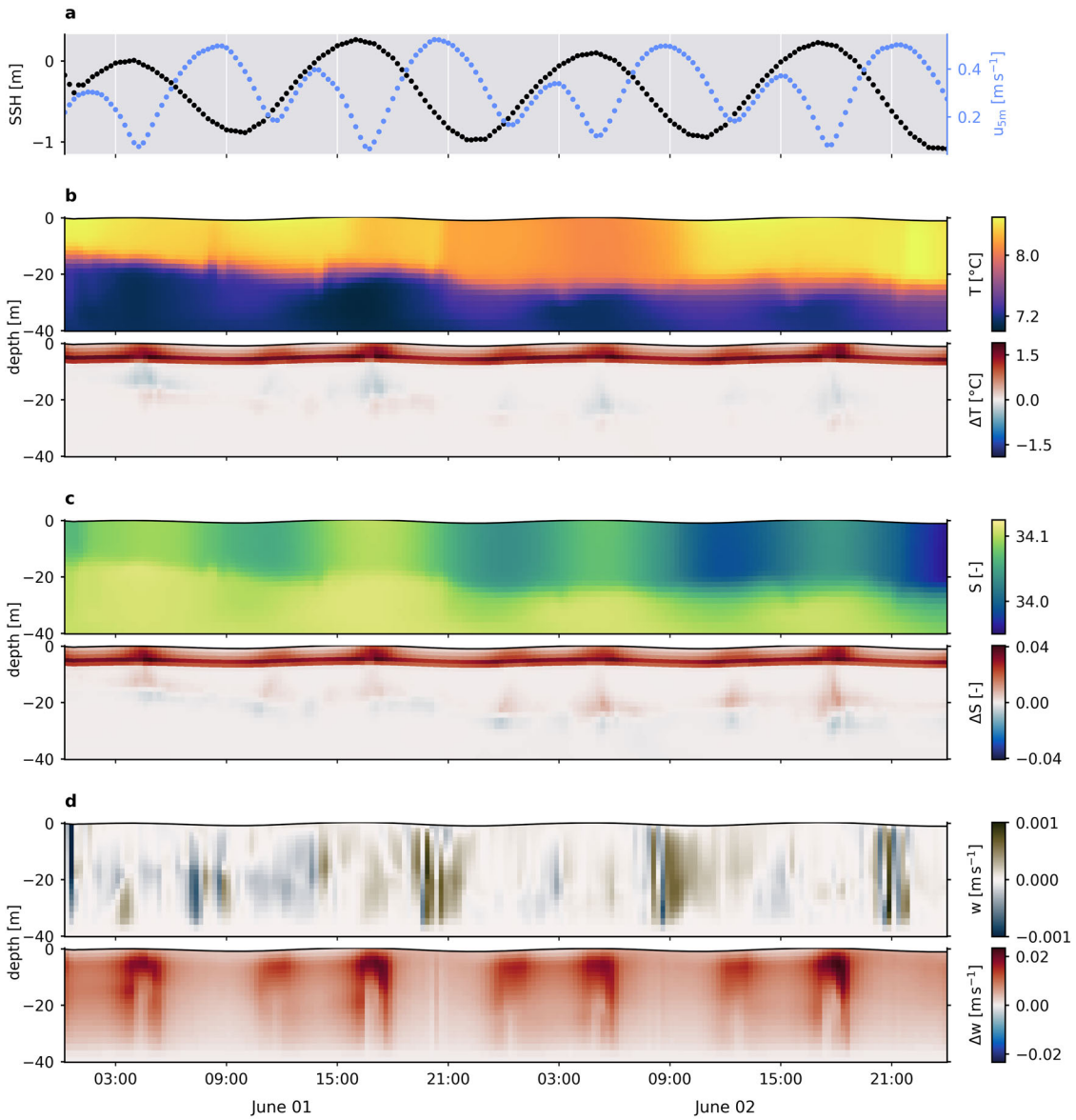

Fig. 3 | Local processes at the discharge location in *SEN-1* over depth and time. **a** Local sea surface height SSH (black dots) and the horizontal velocity u_{5m} inside the grid cell at 5 m depth (blue dots) in the control simulation (*NEST5*). **b** Reference conditions and the associated changes in temperature T due to discharge of waste heat and brine at 500 MW capacity. **c** Reference conditions and associated changes in salinity S. **d** Reference conditions and associated changes in vertical velocity w.

by vertical gradients in temperature and salinity (Fig. 7a). To quantify the strength of the vertical stratification, we use the potential energy anomaly (PEA) here (see Simpson and Bowers, 1981[35]). Adding additional heat close to the surface increases the temperature gradients throughout the water column, while the high salinities induce a vertical density flux towards bottom layers. However, due to the higher volume fluxes associated with waste heat compared to brine, the surface discharge scenario is determined by temperature effects and therefore leads to an increase in stratification near the hydrogen plant (Fig. 7b).

At horizontal model discretization of 100 m, initial surface discharge related to a 500 MW production capacity increases temperature by about 0.3 °C and salinity by about 0.007 (Fig. 7b). While only representing a snapshot of the associated processes, these values emphasize the numerical dilution of the coarser grid resolution in *NEST80*, which underestimates the initial changes by about 10% compared to *NEST5* (see Fig. 3b, c), corresponding to the increase in grid spacing from 10 to 100 m. On the simulated 7-day average of *NEST80*, local changes in stratification can be observed at *SEN-1*, which spread throughout the wind farm area. For the surface discharge scenario, stratification increases by up to 6.5% near the discharge location, with only minor changes of less than 1% exceeding the wind farm boundaries (Fig. 7b).

To investigate strategies for minimizing the local impact on stratification, other discharge scenarios are evaluated in the following. For example, splitting the discharge spatially to two discharge sources could mitigate the impact by 50%, but also enlarges the affected area (Fig. 7c). Other possibilities include discharging temperature and salinity at greater water depths, e.g. near the seabed or distributed vertically. However, we observe even stronger PEA changes for near-bottom discharge of waste heat and brine. For instance, while discharge of high-saline brine would be less influential in the denser deep waters, it amplifies the vertical stratification strength by up to 7.6% (Fig. 7d). Moreover, releasing both heat and brine near the seabed causes the strongest impact on stratification, with a decrease in PEA of 8.6% locally, and likely creates strong buoyancy fluxes due to the large volume of high temperature in the colder bottom layers (Fig. 7e). Instead, discharge distributed equally over the water column proves to be a suitable method to minimize local impact on stratification. Here, concentrations increase almost constantly over depth by less than 0.05 °C and 0.001, respectively, therefore barely

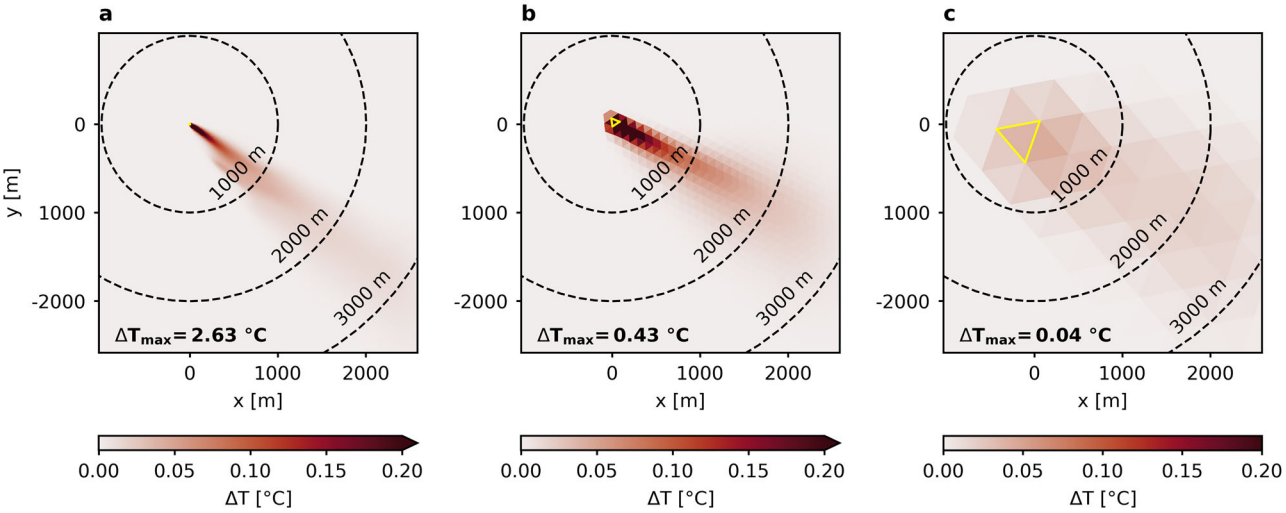

Fig. 4 | Comparison of temperature changes at 5 m depth for different temporal and spatial resolutions. a Temperature plume simulated in *NEST5*. **b** Temperature plume simulated in *NEST80*. **c** Temperature plume simulated in *SEN1*. Panels show a snapshot after three hours. Black dashed circles indicate distances from the discharge source in meters. Yellow triangles illustrate the respective grid cell that contains the source.

affecting the vertical gradients and resulting in PEA changes of just -1.3% on a 7-day average (Fig. 7f).

Over time, the temperature and salinity changes are distributed within *SEN-1*, creating an impact on the local environment that is determined by the waste heat released near the sea surface. However, on the scale of the wind farm area, the strong density changes dissipate quickly and dilute with the ambient seawater. For the *SEN1* configuration, mean surface temperature changes of 0.01 °C in summer extend a few kilometers around the hydrogen plant, affecting an area of approximately 22 km^2 at the initial production capacity of 500 MW (Fig. 8a). Averaged over the model grid cell containing the source (0.108 km^2), local surface temperature increases by about 0.03 °C, while averaged over a radius of 10 km around the hydrogen plant mean temperature changes are below 0.005 °C (Fig. 8b). The production capacity, i.e., the discharge volume, however, has considerable influence on the magnitude of these temperature and salinity anomalies. Thus, at larger capacities of 5 GW or more, the 0.01 °C threshold can extend beyond 25 km distance from the plant, exceeding the wind farm boundaries and affecting areas larger than 1000 km^2. In these cases, local heating in the first square kilometer around the discharge site can reach up to 0.3 °C on average and up to 0.05 °C in a ten-kilometer radius around the source, indicating significant impact on local surface temperature.

Our results clearly illustrate the critical role of production capacity in the impact of a hydrogen plant. To enable estimates of potential hydrographic footprints for future production capacities, we fitted the magnitudes of the mean surface temperature changes as a function of capacity in Fig. 8b. Meanwhile, it should be noted that these area sizes are case-specific and depend on the local environment. In particular, tidal currents and surface winds determine the advection of the surface temperature anomalies and can give different results under different boundary conditions.

Large-scale impact and comparison to offshore wind farm effects

To classify the impact of offshore hydrogen, we compare the magnitude of the temperature changes within *SEN-1* (Fig. 9a) to those resulting from offshore wind farm effects, namely from monopile-induced turbulence (Fig. 9b) and wind speed reduction (Fig. 9c). Starting with a single production site, we assume a capacity of 1 GW for *SEN-1*, as projected in current development plans (https://aquaventus.org/en/, accessed in July 2024). Although the parameterizations for wind farm effects used in this study are generally independent of capacity, the assumed turbine spacing of 1000 m results in 85 turbines in *SEN-1*, yielding an individual turbine capacity of 11.8 MW for a total capacity of 1 GW, which aligns well with the projected

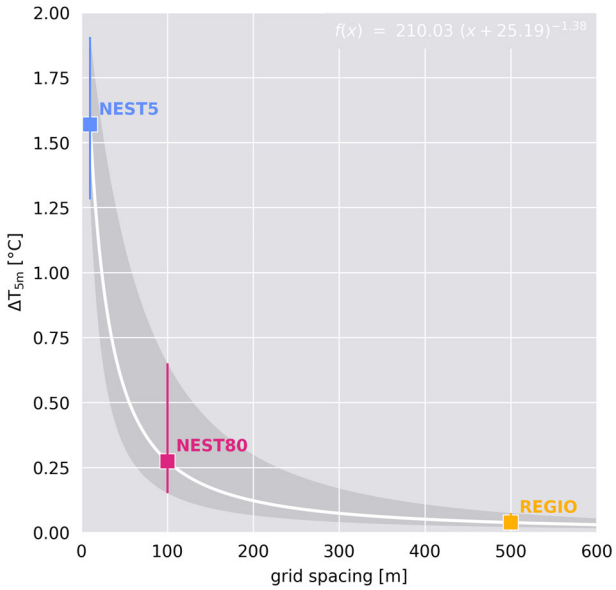

Fig. 5 | Simulated changes at 5 m temperature T_{5m} as a function of the model grid spacing at 500 MW capacity. The colored squares show the changes at the discharge source averaged over two days, with the vertical bars indicating the maximum and minimum changes during that period. The white line shows the fitted function f(x), with the equivalents for maximum and minimum values indicated by the gray area.

average capacity for future offshore wind turbine installations in German waters[36].

The 3-month average shows that offshore hydrogen creates a localized impact on sea surface temperature, with only minor larger-scale effects (Fig. 9a). At a capacity of 1 GW, we observe maximum (numerically diluted) amplitudes of up to 0.07 °C near the hydrogen plant and negligible changes below 0.01 °C outside the wind farm area. In contrast, the effects of the wind farm itself show more extensive effects on surface temperature. On the one hand, the turbulence created by the drag of the wind turbine foundations induces strong vertical mixing that weakens stratification inside the wind farm boundaries. Here, the mixing leads to a decrease in surface temperature of up to 0.1 °C (Fig. 9b). On the other hand, wind speed reduction has been shown to develop on larger scales due to the extent of the atmospheric wind farm wakes[19,26]. Thereby, the reduced surface mixing leads to higher surface

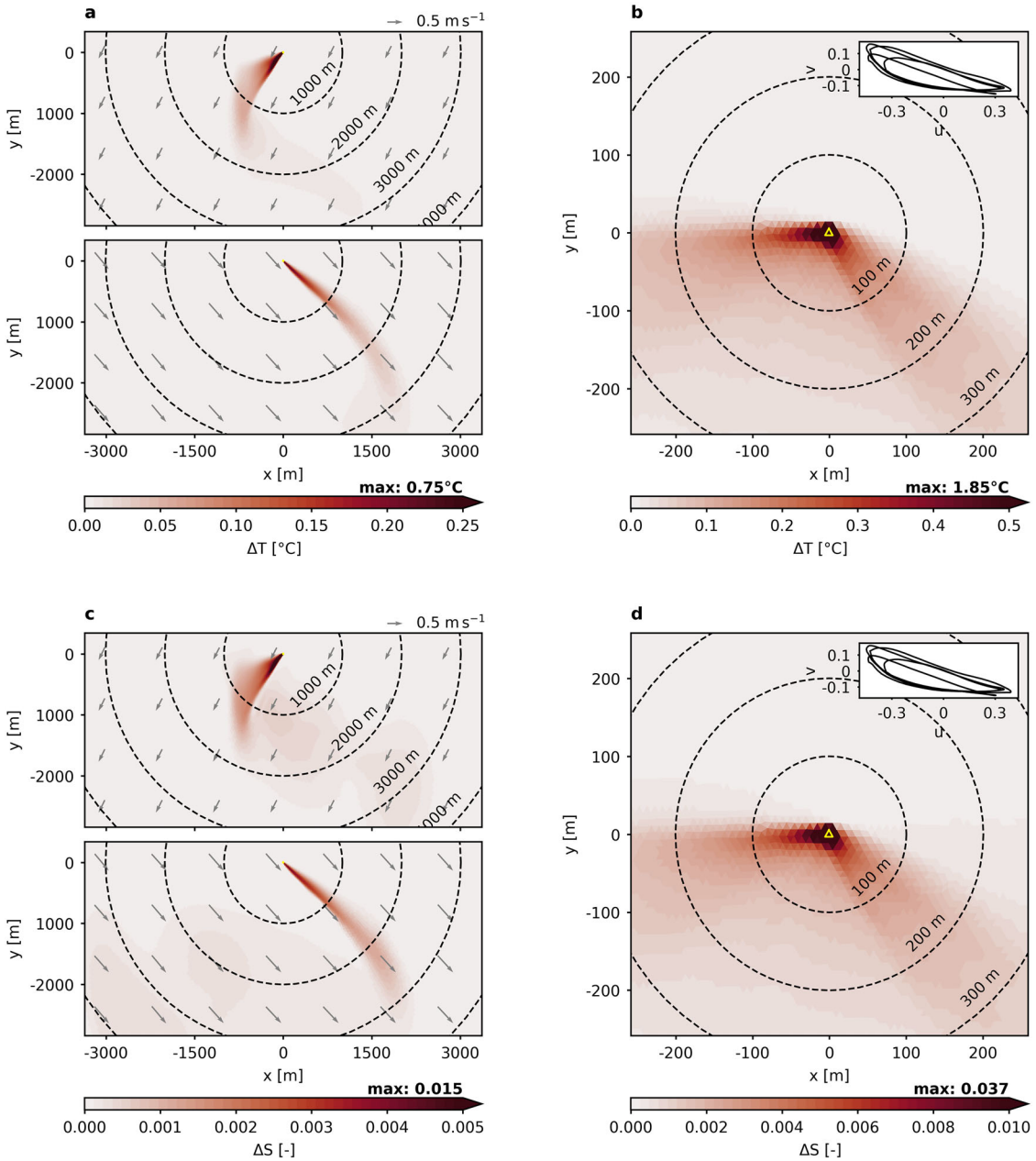

Fig. 6 | Temperature and salinity plumes around the discharge location in *NEST5*. **a** Snapshots of temperature plumes after 6 hours (upper panel) and 14 hours (lower panel). The gray arrows indicate the horizontal surface velocity. **b** Maximum temperature changes over the vertical dimension on the 2-day average. Small panel show the magnitudes of the velocity components u, v during the simulated period in m s^{-1}. **c** Snapshots of salinity plumes after 6 hours (upper panel) and 14 hours (lower panel). The gray arrows indicate the horizontal surface velocity. **d** Maximum salinity changes over the vertical dimension on the 2-day average. In all panels, black dashed circles indicate distances from the discharge location in meters. Yellow triangles illustrate the respective grid cell that contains the source. Colorbars are limited to 30% of the maximum values to enhance visibility.

temperatures in the vicinity of the wind farm. Here, we observe only small changes of about 0.02 °C within the wind farm boundaries (Fig. 9c), as the wind wake parameterization was only applied in the lee of *SEN-1*.

Although far-field effects from offshore hydrogen appear negligible, questions remain about regional implications of potential future development scenarios. Here, we highlight the impact of 10 GW hydrogen production in the German Bight in combination with offshore wind farm effects over a period of one year. To decompose the impact of offshore hydrogen and offshore wind, we ran three simulations: (i) a simulation that considers the projected 10 GW of hydrogen production, (ii) a simulation that takes into account wind farm effects in combination with the 10 GW hydrogen production, and (iii) a simulation that considers the projected 10 GW of hydrogen production plus 70 GW of offshore wind (Fig. 10).

The near-surface discharge from offshore hydrogen production increases the local surface temperature by an annual average of up to 0.2 °C in the vicinity of the hydrogen plants (Fig. 10a). Note that these changes are strongly diluted by the numerical discretization (500 m) and are expected to be at least an order of magnitude larger within 10's of meters around the discharge location (Fig. 5). Near the clustered production sites in the northwest of the German Bight, far-field temperature anomalies occur, but with small values of around 0.01 °C that extend a few tens of kilometers along the residual current. Significant temperature changes remain very localized around the discharge locations. The higher surface temperatures

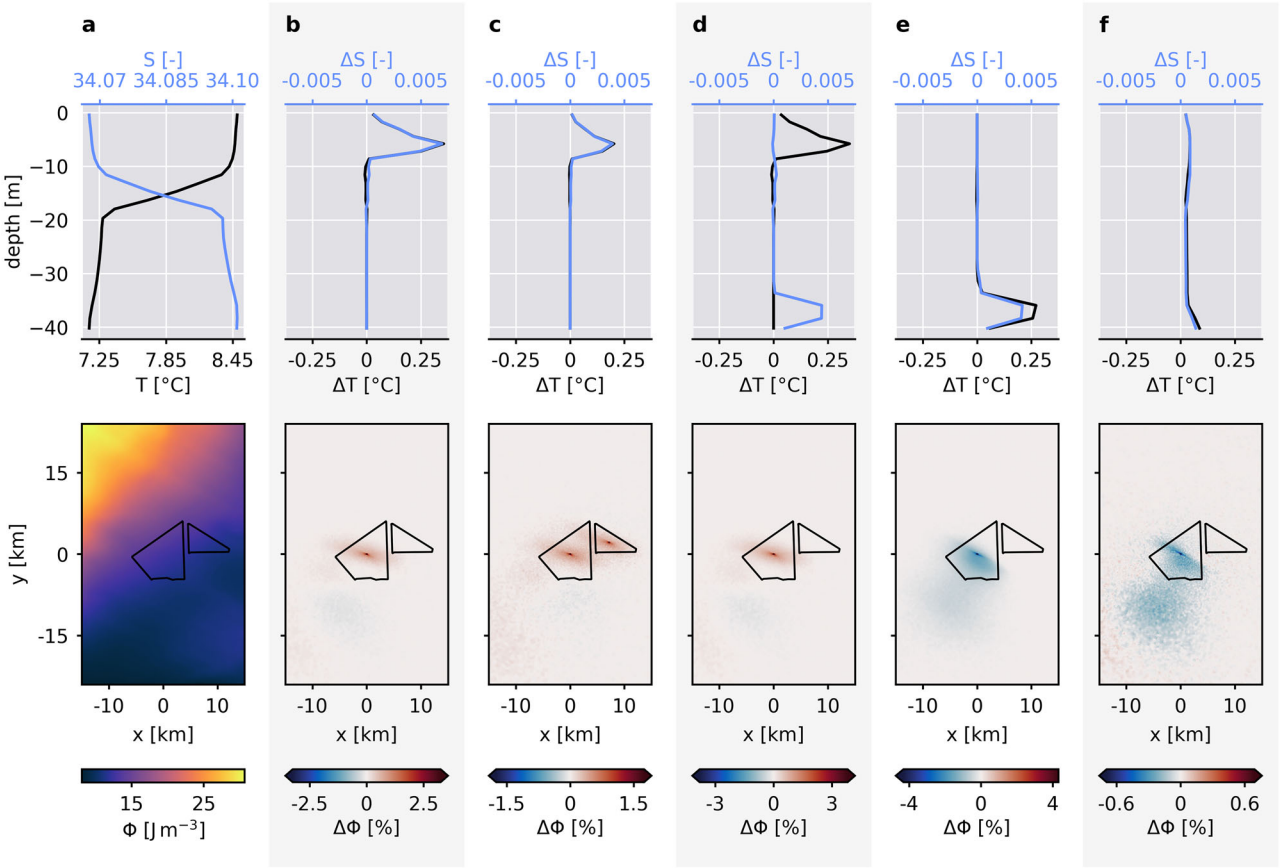

Fig. 7 | Stratification changes due to different discharge scenarios. Upper panels show the vertical changes in temperature T and salinity S at the production site due to the release of waste heat and brine after 30 minutes. Lower panels show the associated percentage changes in potential energy anomaly Φ averaged over the simulated 7-day period in NEST80. **a** Reference conditions from the control simulation. **b** Perturbations due to discharge at 5 m depth; **c** discharge in 5 m splitted horizontally; **d** discharge splitted vertically with waste heat in 5 m and brine in 35 m; **e** discharge at 35 m depth; **f** discharge distributed over depth. Intake of seawater is kept at 10 m depth for all scenarios. The colorbars for potential energy anomaly changes are limited to 50% of the maximum values to enhance visibilty of the effects.

lead to an increase in stratification strength within hydrogen production sites, which displays a seasonality in magnitude that closely aligns with the stratification development over the year (Fig. 10d). Thereby, the changes are expectedly low during winter months, where wind and tides mix the water column, but increase in spring with the onset of stratification. During the summer season, the emitted high temperatures enhance the existing stratification, with average changes within the production sites of around 0.5 J m^{-3}.

In contrast, including offshore wind farm effects to the simulations increases the impact on surface temperature significantly (Fig. 10b, c). Likely driven by the large-scale wind speed reductions, the wind farms cause extensive surface heating within the German Bight, with magnitudes around 0.2 °C. We observe that locally the effects from offshore hydrogen amplify these magnitudes within the wind farms, leading to changes in surface temperature of up to 0.4 °C in areas around the assumed hydrogen plants. While we do not discuss the effects of offshore wind farms on hydrodynamics in more detail here (see Christiansen et al., 2022[19], 2023[24]), we observe that the local changes averaged over the respective hydrogen production sites can reach up to ±7 J m^{-3}, and thus become an order of magnitude larger than the changes associated with hydrogen production (Fig. 10d). Thereby, the changes in PEA show a seasonal trend that counteracts the rising and falling of the stratification development.

Discussion

The cross-scale influence of offshore hydrogen discharge complicates its accurate representation in numerical models. Using high-resolution modeling, we found that significant impact on stratification remains within 100's of meters around the discharge site. Here, we defined a limit for horizontal resolution at about 10 m to not push the boundaries of the hydrostatic model assumptions too far. However, numerical dilution has been shown to have a strong influence on the simulated magnitudes and should be accounted for when interpreting the model results. Coarse grid resolution can lead to considerable loss of magnitude information, while the larger grid spacing increases the horizontal diffusion of the temperature and salinity signals.

To explore the local plume dispersion and vertical mixing processes in more detail, we recommend the use of very high-resolution modeling, such as Large Eddy Simulations (LES), which allows for adequate representation of the non-hydrostatic processes around the discharge site while keeping the numerical dilution to a minimum. The LES approach has been used in earlier studies on brine discharge from seawater desalination plants[37]. Here, however, we focused on regional hydrostatic models to highlight the large-scale effects of offshore hydrogen discharge. Using regional modeling illustrates how the density anomalies propagate in the system, thereby providing valuable insights into the potential extent of the offshore hydrogen footprint. In this context, tides and atmospheric conditions are decisive for advection processes.

In addition to the numerical limitations, uncertainties remain about the impact of offshore hydrogen due to production technologies, degradation/efficiency, and environmental conditions, which affect the volume fluxes and discharge concentrations. This applies in particular to technological aspects such as brine concentration or cooling water requirements,

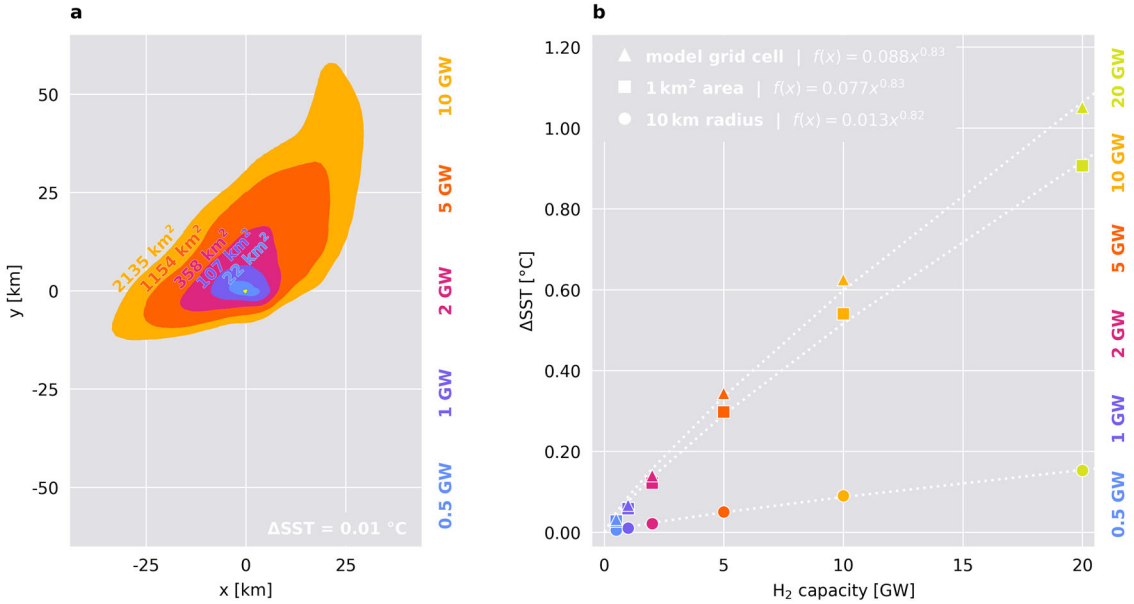

Fig. 8 | Influence of production capacity on the magnitude of temperature anomalies. a Horizontal extent of the areas around *SEN-1* that are affected by a change of at least 0.01 °C in sea surface temperature, averaged over the summer months (June-August, *SEN1*). Colors indicate the different H_2 capacities. Yellow triangle illustrates the location of the source. Black polygons represent *SEN-1*. **b** Horizontally averaged changes in sea surface temperature SST within the grid cell containing the point source (triangles), within 1 km^2 around the source (squres), and within a 10 km radius around the source (circles) as a function of the H_2 capacity. Colors indicate the different H_2 capacities. The dotted white lines show the fitted functions f(x).

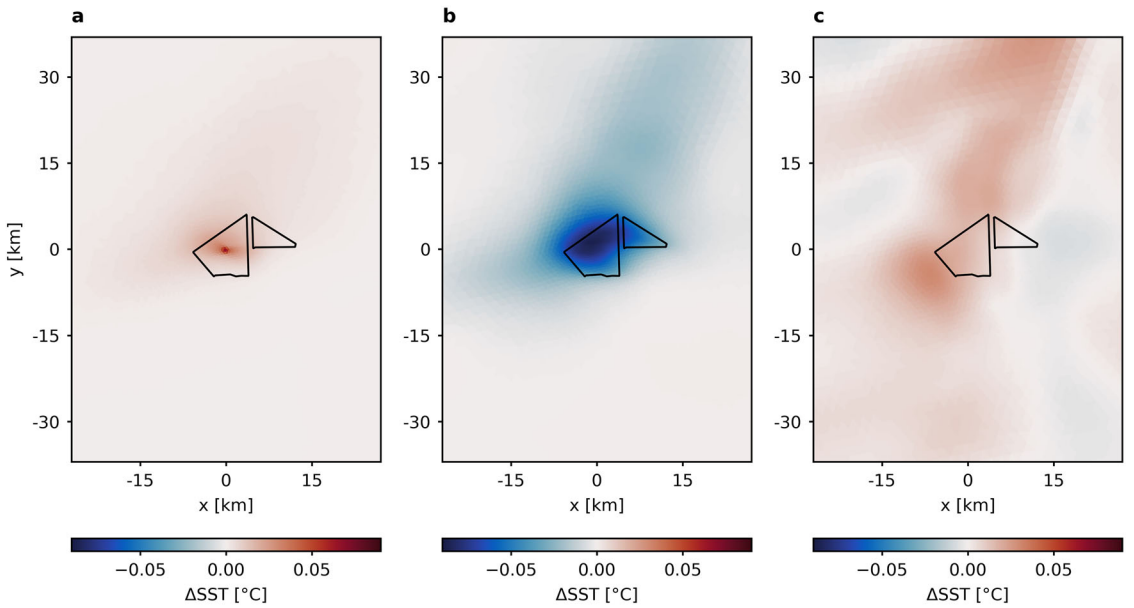

Fig. 9 | Comparison of the impact on mean sea surface temperature SST in the vicinity of *SEN-1*. a Changes in SST caused by 1 GW hydrogen production averaged over three months of simulation (June-August; *SEN1*). **b** Changes in SST caused by monopile-induced drag and turbulence. **c** Changes in SST caused by wind speed reduction. Black polygons indicate *SEN-1*.

with the latter proving to be most influential in this study. To date, most available literature is gray literature or based on theoretical assumptions, but more technological details from industry are needed for an accurate representation of seawater usage and discharge. This also requires strategies and regulations from authorities to guide industry to specify their technology for offshore applications.

The discharge from hydrogen production can generate considerable density anomalies in the vicinity of offshore production sites, with consequences for physical and biogeochemical processes. With the proposed discharge in near-surface layers, we find that the released waste heat is the determining factor for environmental impacts. Here, we identified an area of 50-100 m around the discharge location being exposed to critical temperature changes, assuming a production capacity of 500 MW. Thereby, larger production capacities can enlarge the magnitude as well as the radius of the critical area. While our simulations show an increase in sea surface temperature at the production site of up to 2 °C at 10 m grid spacing, potential future production capacities of 2 GW could amplify the magnitude of temperature changes by a factor of four (Fig. 8). These localized anomalies not only exceed the natural variability of around 1 °C[34] in the southern North Sea but are comparable to or even larger than projected future climate changes in surface temperature of about 1-3 °C[38,39].

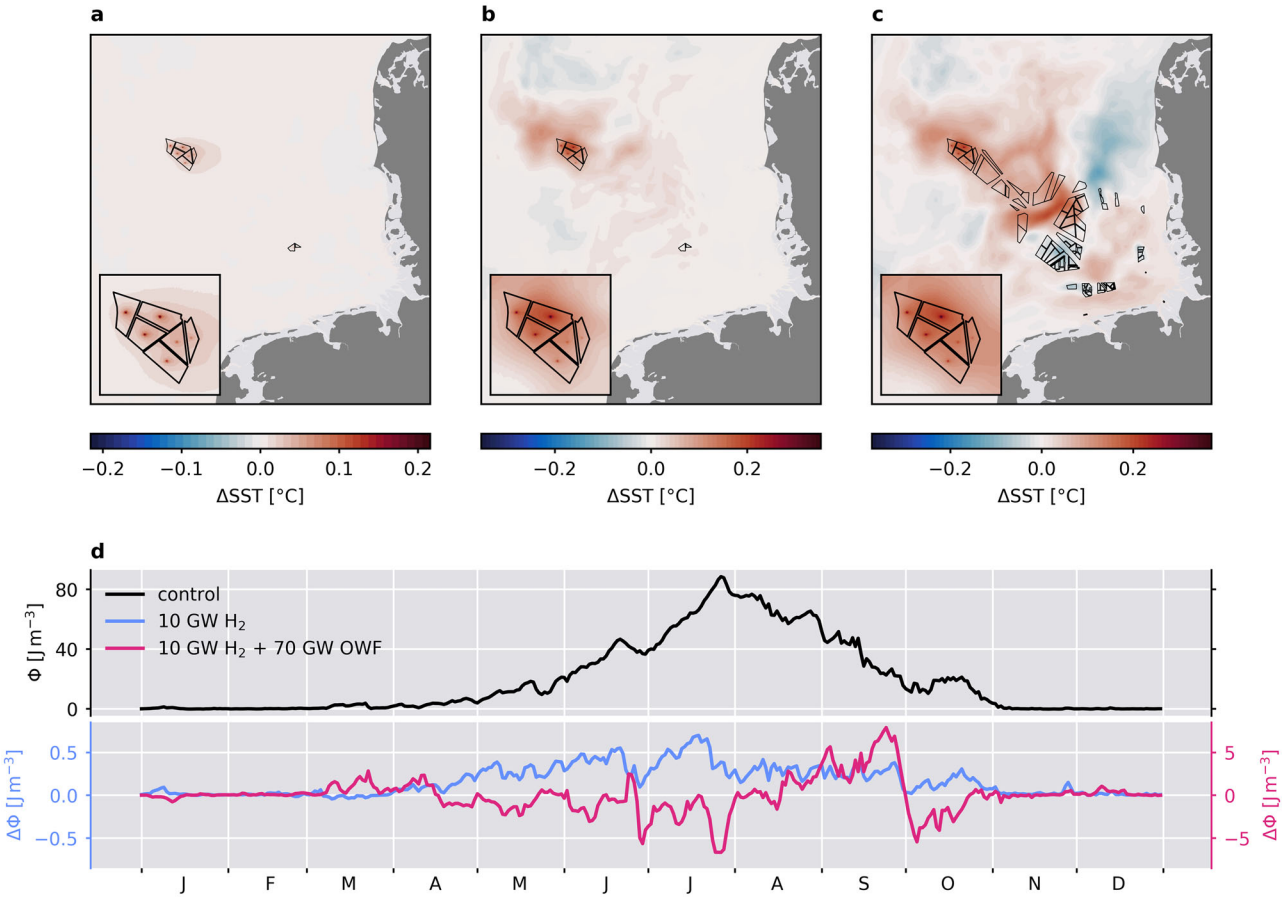

Fig. 10 | Impact on annual mean surface temperature SST in the German Bight due to a hypothetical 2050 offshore renewable energy scenario. a Changes in SST due to 10 GW H_2 production. Black polygons indicate the respective wind farm areas of the 2050 scenario used for the experiment. Small panel highlights the clustered production sites in the northwest of the German Bight. **b** Changes in SST due to 10 GW H_2 production in combination with the effects from the offshore wind farm installations. **c** Changes in SST due to 70 GW offshore wind farms (OWF) in addition to 10 GW H_2 production. **d** Development of the potential energy anomaly Φ (black line) and its disturbances due to the respective scenarios (blue, magenta lines) over the course of one year. The time series are calculated from the horizontally averaged Φ values across the designated hydrogen production sites in each scenario (yellow areas in Fig. 2a).

Rising sea surface temperature due to climate change has been directly linked to intensified stratification in the northwest European shelf[40], with potential increases in potential energy anomaly of 20-40%[39]. While offshore hydrogen production alone is estimated to increase the potential energy anomaly by only 1% on spatial average (Fig. 10d), the observed temperature changes of 2 °C or more in direct vicinity of hydrogen plants suggest an effect on stratification comparable to that of the climate signal. However, the impact on vertical transport might unfold differently here, as we observed strong upwelling associated with the near-surface discharge (Fig. 3d), which is in contrast to the balance between surface heating and mixing as it has been shown for climate change[40].

Strong heating around a hydrogen production site will have consequences for the local marine environment. As mentioned by Lattemann and Höpner (2008)[7], marine organisms can adapt to minor deviations or temporary extremes in temperature and salinity, but the exposure to the continuous discharge from offshore hydrogen production could likely create unfavorable conditions around a hydrogen plant. Depending on species-specific thresholds, the discharge from offshore hydrogen could thus lead to a localized shift or displacement of marine communities and species. For instance, long-term changes in sea surface temperature have been shown to affect the distributional range of the prevailing species communities, e.g., macrobenthos, in the North Sea[41]. Further research is needed to investigate these hypotheses. While we have focused our analysis on waste heat and brine, we neglected other potential by-products like oxygen, operational materials, or cleaning chemicals[7]. In particular, the disposal of chemicals could become critical to marine life and should be addressed in future studies and development.

With increasing distance from the source, the discharge anomalies have been shown to dilute rapidly. The dilution of the initial concentration and thus the impact on the surrounding seawater turned out to be dependent on the prevailing current velocities and ambient mixing rates. At low velocities, where turbulence levels and advection are weak, temperature and salinity changes are much more pronounced. At high velocities, instead, lateral dispersion of the signals is stronger and thus the concentrations dilute faster. We expect less impact from offshore hydrogen in hydrodynamically active regions, where the tides dilute the density plumes rapidly, whereas in regions that are less dominated by tides the impact is expected more significant. For low tidal velocities, we have shown that the density anomalies can generate vertical upwelling of about 0.02 m s^{-1}, which is one order of magnitude larger than the ambient vertical velocity and therefore implies substantial consequences for local stratification or vertical transport, e.g., of nutrients. The strong upwelling caused by the high temperature and high salinity near the sea surface mimics the effects of perpetual salt fountains[42,43], which have been discussed in the context of artificial ocean farming by bringing nutrient-rich deep water to the surface. Thus, emerging upwelling due to surface discharge could create positive impact on local nutrient availability and productivity near the production site.

In most future applications, offshore hydrogen production will be accompanied by offshore wind turbines that supply the electricity required for desalination and electrolysis. Consequently, physical effects caused by

the wind turbines, such as local turbulence due to monopile drag, may interfere with the discharged density anomalies. For instance, enhanced turbulence levels inside offshore wind farms could increase the dilution of the temperature and salinity signals. Surface heating by offshore hydrogen counteracts the turbulence-induced destratification due to turbine foundations but has been shown to amplify the increase in surface temperature due to large-scale wind speed reductions locally (Fig. 10c). The individual interactions between these effects will depend on environmental conditions and the distance between hydrogen plants and wind turbines. Ultimately, we conclude from the high-resolution modeling that the footprint from waste heat and brine in the critical area around a hydrogen plant will be significantly stronger than the impact of offshore wind turbines.

With greater distance from the discharge sites, we observe that wind farm effects determine the impact on temperature and stratification. The far-field effects from offshore wind farms create a much larger spatial influence on surface temperature, thereby affecting regional hydrodynamics. For a potential 2050 German Bight scenario, we show that averaged over offshore hydrogen production sites, the impact of discharge on density stratification accounts for only 10% of the impact from offshore wind farms, specifically wind speed reduction and local turbulence, and appears negligible in the far-field of hydrogen plants. Here, the wind farm effects superimpose the effects from hydrogen discharge, not only because of their magnitudes but also because offshore wind energy development has much higher capacity targets than offshore hydrogen production. Consequently, offshore wind energy is expected to remain determining for the anthropogenic impact on the North Sea, while we suggest that offshore hydrogen will create significant localized footprints on sea temperature, salinity, and stratification. However, note that future developments in offshore wind installations could reduce the effects of wind turbines on surface wind speeds and potentially induced turbulent mixing due to increased turbine spacing with larger wind turbines[44].

As the regional impact turned out minor, questions remain about mitigation strategies for local effects from offshore hydrogen production. Ultimately, industrial development has the biggest potential to minimize the environmental impact by reducing the discharge concentrations or targeting their rapid diffusion. Dewar et al. (2022)[10] showed previously that the discharge depth is one of the major factors to reduce the impact on stratification, while Wood et al. (2020)[9] noted that premixing the brine with cooling water could compensate for strong negative buoyancy fluxes. Here, we demonstrate that vertical and spatial distribution of the discharge volume can reduce the impact on stratification significantly, although increasing the area that is affected by density anomalies. Additionally, artificial mixing or diffuser systems could be installed to increase the dilution of waste heat and brine[5,7]. A potential solution could be to locate offshore hydrogen production close to or mounted on the foundations of offshore wind turbines, i.e., a decentralized approach with integrated electrolysis systems at each individual wind turbine. This approach could not only reduce the amount of individual discharge volumes, thus mimicking the spatial distribution, but also could utilize the strong turbulent mixing at the turbine foundations to intensify diffusion of temperature and salinity anomalies.

Another opportunity is mitigating the discharges through technological development, e.g., reducing or avoiding the discharge of waste heat and brine into the sea. Electrolysis technologies like AEL or PEMEL show efficiencies of around 60%[14], meaning that 40% of energy gets lost or discharged through waste heat. Increasing the efficiency or utilizing the waste heat as energy sources, as it is already done in desalination methods like MED, could thus be promising solutions to mitigate the impact on surface temperature.

The main impact of an offshore hydrogen plant, however, results from the seawater treatment used for desalination. In this study, we focused on thermal desalination processes in form of MED. These methods have high water demands and create a thermal footprint on the environment due to large amounts of waste heat[6,15], which turned out to be the crucial factor in this study. The thermal footprint of hydrogen plants could be reduced by using membrane processes like Reverse Osmosis instead. RO proves to be more energy efficient and can reduce the water demand of a hydrogen plant[6,15]. However, the membrane processes could increase the saline and chemical footprint of the water treatment. Further investigations are needed to directly compare the hydrographic footprint of state-of-the-art thermal and membrane processes. This also includes the consideration of chemical by-products and their impact on the marine ecosystem.

Conclusion

Offshore hydrogen production, more specifically the discharge of waste heat and brine into the sea, can have significant impact on the marine environment within 10's to 100's of meters around the production sites. Local temperature and salinity anomalies can become substantial for marine organisms by creating unfavorable conditions, however, more high-resolution modeling of plume dispersion is needed to understand these processes properly, including a range of different hydrodynamic and weather conditions. Our models indicate that the discharge from offshore hydrogen production, especially waste heat, can cause significant surface heating around hydrogen plants that exceeds long-term natural variabilities and projected climate change signals. Here, we showed that the choice of the discharge depth determines the impact on stratification. While surface discharge turned out to be less impactful than bottom discharge, horizontal and vertical distribution of the discharge fluxes might help to reduce environmental implications. Tidal dispersion is crucial for rapid dilution of the generated density anomalies, but also technological aspects like the production capacity determine the magnitude of the hydrographic footprint. Further research is needed on the local biogeochemical impact of discharged by-products or harmful chemicals that enter the sea with the brine.

With increasing distance from the hydrogen plant, temperature and salinity signals are diluted, which rapidly reduces the impact on stratification. The far-field effects of offshore hydrogen production are small for expected production capacities below 2 GW, with no significant impact on regional stratification. Especially when accompanied by offshore wind farms, the latter are decisive for the hydrographic footprint of offshore hydrogen production. Nevertheless, our findings indicate that future offshore hydrogen production can increase the local annual mean sea surface temperature by up to 0.2 °C within a range of 500-1000 meters from the production sites. Production capacities of more than 2 GW could intensify these effects considerably. To mitigate the impact on the local environment, our results suggest spreading the disposal of waste heat and brine spatially, for example by employing decentralized low-capacity plants at each wind turbine.

Data Availability

The datasets used and analyzed in the current study are available from the corresponding author on reasonable request.

Received: 6 August 2024; Accepted: 17 April 2025;
Published online: 06 May 2025

References

1. IEA. *Key World Energy Statistics 2021*. https://www.iea.org/reports/key-world-energy-statistics-2021 (2021).
2. European Commission. *A Hydrogen Strategy for a Climate-Neutral Europe*. https://eur-lex.europa.eu/legal-content/EN/ALL/?uri=CELEX:52020DC0301 (2020).
3. WindEurope. *Offshore Wind in Europe: Key Trends and Statistics in 2020*. https://windeurope.org/intelligence-platform/product/offshore-wind-in-europe-key-trends-and-statistics-2020/ (2021).
4. van Medevoort, J., Kuipers, N. & ten Hoopen, P. Hydrogen from seawater via membrane distillation and polymer electrolyte membrane water electrolysis (SEA2H2). https://www.wur.nl/en/project/hydrogen-from-seawater.htm (2022).

5. Rudolph, A. et al. *Projekt OffsH2ore - Offshore-Wasserstofferzeugung Mittels Offshore-Windenergie Als Insellösung (Endbericht)*. https://www.ise.fraunhofer.de/de/forschungsprojekte/offsh2ore.html (2023).
6. D'Amore-Domenech, R. & Leo, T. J. Sustainable Hydrogen Production from Offshore Marine Renewable Farms: Techno-Energetic Insight on Seawater Electrolysis Technologies. *ACS Sustain Chem. Eng.* **7**, 8006–8022 (2019).
7. Lattemann, S. & Höpner, T. Environmental impact and impact assessment of seawater desalination. *Desalination* **220**, 1–15 (2008).
8. Rodenburg, J. et al. North Sea Energy—Safety Integrity & Reliability of offshore hydrogen production installations. https://north-sea-energy.eu/static/0188ffe57ce1218a84615b6955109341/NSE-2020-2022-3-Safety-Integrity-Reliability-of-offshore-hydrogen-production-installations.pdf (2022).
9. Wood, J. E., Silverman, J., Galanti, B. & Biton, E. Modelling the distributions of desalination brines from multiple sources along the Mediterranean coast of Israel. *Water Res.* **173**, 115555 (2020).
10. Dewar, M., Blackford, J., Espie, T., Wilford, S. & Bouffin, N. Impact potential of hypersaline brines released into the marine environment for CCS reservoir pressure management. *Int. J. Greenh. Gas. Control* **114**, 103559 (2022).
11. Roberts, D. A., Johnston, E. L. & Knott, N. A. Impacts of desalination plant discharges on the marine environment: A critical review of published studies. *Water Res.* **44**, 5117–5128 (2010).
12. Simpson, J. H. & Sharples, J. *Introduction to the Physical and Biological Oceanography of Shelf Seas*. (Cambridge University Press, Cambridge, 2012). https://doi.org/10.1017/CBO9781139034098.
13. Carmo, M., Fritz, D. L., Mergel, J. & Stolten, D. A comprehensive review on PEM water electrolysis. *Int J. Hydrog. Energy* **38**, 4901–4934 (2013).
14. Buttler, A. & Spliethoff, H. Current status of water electrolysis for energy storage, grid balancing and sector coupling via power-to-gas and power-to-liquids: A review. *Renew. Sustain. Energy Rev.* **82**, 2440–2454 (2018).
15. Ghaffour, N., Missimer, T. M. & Amy, G. L. Technical review and evaluation of the economics of water desalination: Current and future challenges for better water supply sustainability. *Desalination* **309**, 197–207 (2013).
16. Zhang, Y. J., Ye, F., Stanev, E. V. & Grashorn, S. Seamless cross-scale modeling with SCHISM. *Ocean Model ((Oxf.))* **102**, 64–81 (2016).
17. Umlauf, L. & Burchard, H. A generic length-scale equation for geophysical turbulence models. *J. Mar. Res* **235**, 265 (2003).
18. Zhang, Y. J., Stanev, E. V. & Grashorn, S. Unstructured-grid model for the North Sea and Baltic Sea: Validation against observations. *Ocean Model ((Oxf.))* **97**, 91–108 (2016).
19. Christiansen, N., Daewel, U., Djath, B. & Schrum, C. Emergence of Large-Scale Hydrodynamic Structures Due to Atmospheric Offshore Wind Farm Wakes. *Front. Mar. Sci*. **9**, 818501 (2022).
20. Helmholtz-Zentrum Geesthacht, Zentrum für Material- und Küstenforschung GmbH (HZG). coastDat-3_COSMO-CLM_ERAi. World Data Center for Climate (WDCC) at DKRZ. http://cera-www.dkrz.de/WDCC/ui/Compact.jsp?acronym=coastDat-3_COSMO-CLM_ERAi (2017).
21. Rakovec, O. & Kumar, R. Mesoscale Hydrologic Model based historical streamflow simulation over Europe at 1/16 degree. World Data Center for Climate (WDCC) at DKRZ. https://doi.org/10.26050/WDCC/mHMbassimEur (2022).
22. Taguchi, E., Stammer, D. & Zahel, W. Inferring deep ocean tidal energy dissipation from the global high-resolution data-assimilative HAMTIDE model. *J. Geophys Res Oceans* **119**, 4573–4592 (2014).
23. Zhang, Y. J., Ateljevich, E., Yu, H.-C., Wu, C. H. & Yu, J. C. S. A new vertical coordinate system for a 3D unstructured-grid model. *Ocean Model ((Oxf.))* **85**, 16–31 (2015).
24. Christiansen, N., Carpenter, J. R., Daewel, U., Suzuki, N. & Schrum, C. The large-scale impact of anthropogenic mixing by offshore wind turbine foundations in the shallow North Sea. *Front. Mar. Sci*. **10**, 1178330 (2023).
25. Rennau, H., Schimmels, S. & Burchard, H. On the effect of structure-induced resistance and mixing on inflows into the Baltic Sea: A numerical model study. *Coast. Eng.* **60**, 53–68 (2012).
26. Ludewig, E. *On the Effect of Offshore Wind Farms on the Atmosphere and Ocean Dynamics*. (Springer Cham, 2015). https://doi.org/10.1007/978-3-319-08641-5.
27. Daewel, U., Akhtar, N., Christiansen, N. & Schrum, C. Offshore wind farms are projected to impact primary production and bottom water deoxygenation in the North Sea. *Commun. Earth Environ.* **3**, 292 (2022).
28. Raghukumar, K. et al. Projected cross-shore changes in upwelling induced by offshore wind farm development along the California coast. *Commun. Earth Environ.* **4**, 116 (2023).
29. van Leeuwen, S., Tett, P., Mills, D. & van der Molen, J. Stratified and nonstratified areas in the North Sea: Long-term variability and biological and policy implications. *J. Geophys Res Oceans* **120**, 4670–4686 (2015).
30. BMWK. Fortschreibung der Nationalen Wasserstoffstrategie. https://www.bmwk.de/Redaktion/DE/Publikationen/Energie/fortschreibung-nationale-wasserstoffstrategie.html (2023).
31. Bundesregierung. Windenergie-auf-See-Gesetz - WindSeeG. https://www.gesetze-im-internet.de/windseeg/index.html (2023).
32. Stoevesandt, B. & Schwegmann, S. *Offshore Flächenpotenziale: Analyse Der Energieerzeugungseffizienz in Der Deutschen AWZ.* https://bwo-offshorewind.de/uberarbeitete-flachenpotenzialstudie-des-fraunhofer-iwes/ (2022).
33. van Wingerden, T., Geerdink, D., Taylor, C. & Hülsen, C. F. Specification of a European Offshore Hydrogen Backbone. https://aquaventus.org/wp-content/uploads/2023/03/DNV-Study_Specification_of_a_European_Offshore_Hydrogen_Backbone.pdf (2013).
34. Daewel, U. & Schrum, C. Low-frequency variability in North Sea and Baltic Sea identified through simulations with the 3-D coupled physical–biogeochemical model ECOSMO. *Earth Syst. Dyn.* **8**, 801–815 (2017).
35. Simpson, J. H. & Bowers, D. Models of stratification and frontal movement in shelf seas. *Deep Sea Res. Part A. Oceanographic Res. Pap.* **28**, 727–738 (1981).
36. Deutsche Windguard. *Status of Offshore Wind Energy Development in Germany - First Half of 2023*. https://www.windguard.com/publications-wind-energy-statistics.html?file=files/cto_layout/img/unternehmen/veroeffentlichungen/2023/Status%20of%20Offshore%20Wind%20Energy%20Development%20in%20Germany_First%20Half%202023.pdf (2023).
37. Zhang, S., Jiang, B., Law, A. W.-K. & Zhao, B. Large eddy simulations of 45° inclined dense jets. *Environ. Fluid Mech.* **16**, 101–121 (2016).
38. Schrum, C. et al. Projected Change—North Sea. In: Quante, M., Colijn, F. (eds) North Sea Region Climate Change Assessment. Regional Climate Studies. Springer, Cham., 175–217. https://doi.org/10.1007/978-3-319-39745-0_6 (2016).
39. Tinker, J., Lowe, J., Pardaens, A., Holt, J. & Barciela, R. Uncertainty in climate projections for the 21st century northwest European shelf seas. *Prog. Oceanogr.* **148**, 56–73 (2016).
40. Holt, J., Harle, J., Wakelin, S., Jardine, J. & Hopkins, J. Why Is Seasonal Density Stratification in Shelf Seas Expected to Increase Under Future Climate Change?. *Geophys Res Lett.* **49**, e2022GL100448 (2022).
41. Kröncke, I. et al. Changes in North Sea macrofauna communities and species distribution between 1986 and 2000. *Estuar. Coast Shelf Sci.* **94**, 1–15 (2011).

42. Stommel, H., Arons, A. B. & Blanchard, D. An oceanographical curiosity: the perpetual salt fountain. *Deep Sea Res. ((1953))* **3**, 152–153 (1956).
43. Maruyama, S. et al. Evidences of increasing primary production in the ocean by Stommel's perpetual salt fountain. *Deep Sea Res. Part I: Oceanographic Res. Pap.* **58**, 567–574 (2011).
44. Akhtar, N., Geyer, B. & Schrum, C. Larger wind turbines as a solution to reduce environmental impacts. *Sci. Rep.* **14**, 6608 (2024).

Acknowledgements

This study is a contribution to the EXC 2037 'Climate, Climatic Change, and Society (CLICCS)' (Project Number: 390683824) funded by the German Research Foundation (DFG), to the CLICCS-HGF networking project funded by the Helmholtz Association of German Research Centers (HGF), and to the Helmholtz Research Program "Changing Earth – Sustaining our Future", Topic 4. The funders played no role in study design, data collection, analysis and interpretation of data, or the writing of this manuscript.

Author contributions

NC, UD, CS conceived the study. NC designed the study setup, performed the model simulations and data analysis, and prepared the manuscript. UD and CS contributed to the data analysis. LK contributed to the theoretical assumptions used in the methodology. All authors contributed to manuscript writing and approved the final version.

Funding

Open Access funding enabled and organized by Projekt DEAL.

Competing interests

The authors declare no competing interests.

Additional information

Supplementary information The online version contains supplementary material available at https://doi.org/10.1038/s44183-025-00121-w.

Correspondence and requests for materials should be addressed to Nils Christiansen.